Available online at www.sciencedirect.com
SCIENCE DIRECT
Polymer 46 (2005) 6666–6681
polymer
www.elsevier.com/locate/polymer

Synthetic aspects and characterization of polypropylene–silica nanocomposites prepared via solid-state modification and sol–gel reactions

Sachin Jain[a,d,*], Han Goossens[a,d], Francesco Picchioni[a], Pieter Magusin[b], Brahim Mezari[b], Martin van Duin[a,c,d]

[a]*Department of Chemical Engineering and Chemistry, Eindhoven University of Technology, P.O. Box 513, 5600 MB Eindhoven, The Netherlands*
[b]*Laboratory of Inorganic Chemistry and Catalysis, Eindhoven University of Technology, P.O. Box 513, 5600 MB Eindhoven, The Netherlands*
[c]*DSM Research, P.O. Box 18, 6160 MD Geleen, The Netherlands*
[d]*Dutch Polymer Institute, P.O. Box 9025600 AX, Eindhoven, The Netherlands*

Abstract

A new route is developed by combining solid-state modification (SSM) by grafting vinyl triethoxysilane (VTES) with a sol–gel method to prepare PP/silica nanocomposites with varying degree of adhesion between filler and matrix. VTES was grafted via SSM in porous PP particles. Bulk polymerization under similar experimental conditions as in SSM resulted in homopolymerization of VTES. However, SEC and NMR experiments showed that VTES was grafted as a single monomeric unit in the amorphous phase of PP with the possibility of VTES–polymer grafting during SSM. Silica-like nano-particles were synthesized in-situ by the sol–gel method. Magic-angle spinning (MAS) ^{29}Si NMR spectra showed that the chemical building blocks of the silica-like clusters are of Q^3 and Q^4 type. MAS ^{29}Si NMR and FT-IR spectroscopy showed that the grafted VTES becomes part of the in-situ formed silica particles. No decrease in molecular weight of PP was observed, indicating that chain scission is marginal compared to melt modification. The morphology of the nanocomposites as observed by ATR-FTIR microscopy showed a uniform dispersion of grafted VTES as well as in-situ formed silica. TEM and SEM demonstrated that the in-situ formed silica particles are nearly spherical and have sizes in the range of 50–100 nm.

Keywords: Hybrid nanocomposites; Solid-state modification; Sol–gel method

1. Introduction

Inorganic particle-filled polymer nanocomposites have attracted great interest over the last decade [1–4]. Recent advances in polypropylene (PP)/clay [5] and PP/silicate [6] nanocomposites have further inspired researchers to synthesize PP-based organic/inorganic nanocomposites [7,8]. The interface between the inorganic particles and the PP matrix plays an important role in dispersing the particles and the properties of composites. Earlier studies showed that debonding is an important mechanism in improving the toughness of particle-filled semi-crystalline polymers, because it allows shear yielding of matrix ligaments between the debonded particles [9]. The interfacial strength affects the debonding process and concomitant delocalization of stresses during the macroscopic deformation [10]. However, most of the studies concerning the mechanism of toughness enhancement were performed on micro-particle filled composites. When the dimension of the fillers is reduced from micro- to nanometer scale the surface-to-volume ratio is increased resulting in improved barrier properties and superior mechanical performance [11]. In the context of optimizing the dispersion of fillers and the interfacial properties, it is important to synthesize inorganic particle-filled PP nanocomposites in which the interfacial strength can be tuned.

Despite many efforts in the past, the conventional routes for preparing such inorganic particle-filled PP nanocomposites have their deficiencies and could not be exploited. Melt

* Corresponding author. Department of Chemical Engineering, University of Groningen, Nijenborgh 4, 9747 AG Groningen, The Netherlands. Fax: +31 40 243 6999.
E-mail address: f.p.picchioni@tue.nl (F. Picchioni).

0032-3861/$ - see front matter © 2005 Elsevier Ltd. All rights reserved.
doi:10.1016/j.polymer.2005.05.021

compounding [12,13], solution blending [14], melt intercalation, in-situ intercalative polymerization [15] are well-studied conventional methods to prepare PP nanocomposites. However, oxidation and β-scission leads to degradation of PP during melt modification/compounding. Solvent removal is another problem faced in some of these methods. These problems add extra parameters, apart from the dispersion of fillers and the interfacial strength, which affect the morphology and the final properties of the PP nanocomposites prepared by these methods.

In view of these problems, we have developed a new strategy to prepare PP nanocomposites by combining solid-state modification (SSM) of PP and the sol–gel method for making organic–inorganic hybrid materials. SSM is a solvent free-method of PP modification largely suppressing oxidation and β-scission [16]. SSM is advantageous due to its inherent simplicity, low temperature and solvent-free reaction conditions. Although the absence of solvent is one of the main advantages of SSM, small quantities may be used as diffusion aid or promoter to increase the grafting efficiency [17,18]. In this study, SSM of PP essentially involves the grafting of polar monomers, which can be subsequently incorporated in in-situ made inorganic particles, thus providing chemical interaction between matrix and filler. Some fundamental aspects of the solid-state grafting onto PP were studied by Rätzsch et al. [19]. An important parameter for SSM of PP is the morphology of nascent PP powder from the polymerization reactor [20]. The actual morphology of such PP powders, prepared by the reactor granular technology, is shown in Fig. 1. The porous macroparticles are composed of many sub-particles, which are also porous. The PP macroparticles are approx. 300 μm. The sub-particles are in the order of 50 μm. The irregular channels between these sub-particles are typically 2–3 μm and the pore sizes are 2 μm at the surface to 500 nm inside the particle.

Hybridization, on the other hand, is a method to produce nano-scale inorganic particles in organic matrices with a good dispersion of the filler in the matrix [21]. The most prevalent and widely used hybridization technique for preparing inorganic particles, like silica, is a sol–gel reaction [22,23]. The sol–gel method utilizes mild synthetic conditions, which allow versatile access to chemically designed organo–inorganic hybrid materials. The process involves the hydrolysis of metal alkoxides, followed by a condensation reaction to produce metal oxides [24].

In this paper we report on the synthetic aspects of inorganic particle-filled PP nanocomposites with focus on the chemical and structural characterization and on the morphology. Two type of PP nanocomposites were prepared using the following approach: (1) PP/silica nanocomposites with physical (weak) interactions; there are no chemical bonds between the filler and the PP matrix; (2) PP-*g*-silane/silica nanocomposites with chemical interactions between the organic PP and the inorganic silica phase; the filler particles are chemically attached to the PP chains.

Solid-state grafting of vinyl triethoxysilane (VTES) on PP enables the interfacial interaction between filler and matrix. Subsequently, the silica-like inorganic nano-particles can be prepared in-situ via the sol–gel method. Grafting of VTES and its influence on the in-situ preparation of PP/silica nanocomposites is investigated and discussed, taking into account the possibility of homopolymerization of VTES, which has been neglected in previous studies [16]. We anticipate that this new approach of combining SSM and hybridization will prove to be effective and instrumental in making model systems to study the improvement in mechanical properties and the underlying local deformation mechanisms of particle-filled semi-crystalline polymers. This approach may help to

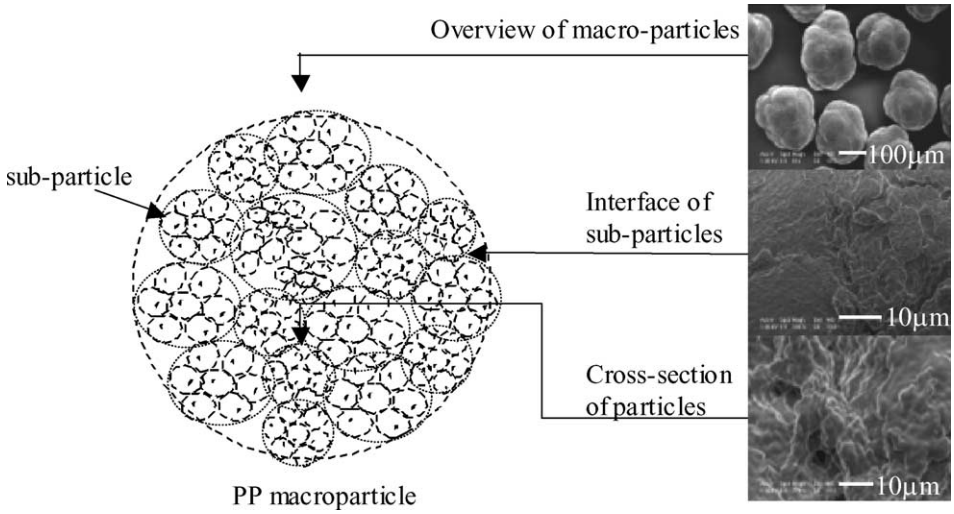

Fig. 1. Morphology of PP macroparticle prepared by reactor granular technology: schematic representation of double grain model and SEM micrographs, showing the morphology of the PP powder used.

overcome the various difficulties faced in the modification of semi-crystalline polymers and of dispersing fillers.

2. Experimental

2.1. Materials

All the chemicals and polymers were used as purchased without any further purification or modification. Porous, isotactic polypropylene (PP) having a porosity of $S_{BET(Kr)} = 0.0678\ m^2/g$ was supplied in powder form by Euro-Sabic, The Netherlands. The weight-average and number-average molecular weight of PP were 400 and 100 kg/mol respectively. The crystallinity of the PP determined from DSC measurements is 60%. The powder was free of antioxidants and stabilizers and was stored at −10 °C in the dark. Vinyl triethoxy silane (VTES) and tetraethoxy orthosilicate (TEOS) were obtained from Aldrich Chemicals. Ammonium hydroxide (NH4OH) [28% NH_3 in water] obtained from Aldrich chemicals was used as catalyst for sol–gel reactions. Various free-radical initiators were selected for grafting based on their chemical structures and half-life times. Di-*tert*-butyl peroxide (DTBP) and α,α′-azoisobutyronitrile (AIBN) from Merck Schuchardt, Germany, dibenzoyl peroxide (BPO) from Fluka Chemicals and lauroyl peroxide (LPO) from Aldrich Chemicals were used as initiators. The half-life time of decomposition at 100 °C for each initiator is: DTBP: 8400 min, BPO: 22 min, AIBN: 7 min, and LPO: 6 min.

2.2. Synthesis of nanocomposites

Picchioni et al. [25] gave a detailed description of the experimental set-up. All reactions were carried out in a double-skinned SSM reactor [26,27]. Hot oil is circulated through the double-skinned jacket to maintain the reaction temperature. The reactor was equipped with a water condenser and a mechanical stirrer. Reactions were carried out under nitrogen flow to have inert atmospheric conditions and to remove traces of oxygen, which otherwise could trigger the oxidation of PP. A peristaltic pump was attached to the reactor to feed the reactive mixture at the desired rate. The feeding rate was calculated from the density of the reactive mixture and the addition time. The flow rate is expressed in pph/min, i.e. parts per hundred of reactive mixture with respect to PP per minute. All the reactions were carried at temperatures below the melting temperature of PP. The nanocomposites and modified PP were obtained from the reactor in powder form. The final products were immediately recovered from the reactor and stored at −4 °C before further characterization.

PP/silica nanocomposites were prepared without chemical modification of PP; PP-*g*-silane/silica nanocomposites involves SSM for VTES grafting, followed by hybridization to make in-situ silica (sol–gel reaction).

2.2.1. PP/silica nanocomposites

PP/silica nanocomposites were prepared by the sol–gel method. TEOS was added to PP in the reactor and stirred for approx. 30 min at 60 °C. After the dispersion of TEOS, a mixture of water and ammonium hydroxide (NH_4OH) was added slowly at a controlled rate to the reactor with continuous stirring. The molar ratio of TEOS/H_2O was 1:5 and NH_4OH was 1 wt% based on TEOS. The sol–gel reaction was carried out in the reactor at 60 °C for 3 h with continuous stirring. The thus formed sol in PP is then gelled at 80 °C for 5 h and dried under vacuum at 120 °C for 24 h. The samples were physically mixed with antioxidants using a powder blender before any further treatment and dried under vacuum at 100 °C before chemical and structural characterization.

2.2.2. PP-g-silane/silica nanocomposites

The first step in the synthesis of PP-*g*-silane/silica nanocomposites was grafting of VTES on PP via SSM as shown in Scheme 1. The free-radical initiator decomposes into free radicals, which initiate the reactions (i) by transferring the radical to the PP backbone and (ii) by addition to the monomer. Part of the monomer may homopolymerize and eventually might graft by a coupling reaction to a PP radical. First, the VTES was dispersed in the pores and subsequently diffuse into the amorphous phase of PP and then the initiator was added slowly, as described in our earlier work on other monomers [25]. The reaction temperature was chosen depending on the decomposition time/temperature of the free radical initiators. The total reaction time was about four times the half-life time of the initiators at the particular reaction temperature. At the end of a reaction, the reactor was heated to higher temperatures to deactivate all the undecomposed initiator. Subsequently, the modified PP was kept under vacuum at approx. 80 °C for 24 h to remove all unreacted monomer and then stored in an airtight desiccator to avoid absorption of moisture. The second step involves the sol–gel process. This can be combined with the first step in the same set-up or separately under other experimental conditions. This step is similar to the formation of silica described above.

The cross-linking of VTES-grafted PP, obtained via melt modification, is a well-studied process used in the cable industry [28]. The cross-linking of VTES-grafted PP involves the formation of Si–O–Si linkages similar those in silica formation. The grafted VTES undergoes hydrolysis followed by condensation in the presence of water vapor at 120 °C forming (Si–O–Si) linkages, which cross-link the grafted PP chains. This reaction is usually carried out at ~100 °C under a nitrogen atmosphere in a closed container. 3 mol of water per mole of grafted VTES is used for the cross-linking reaction. Moreover, if grafted VTES becomes part of the in-situ formed silica during the sol–gel reaction, the surface then resembles the cross-linked structures.

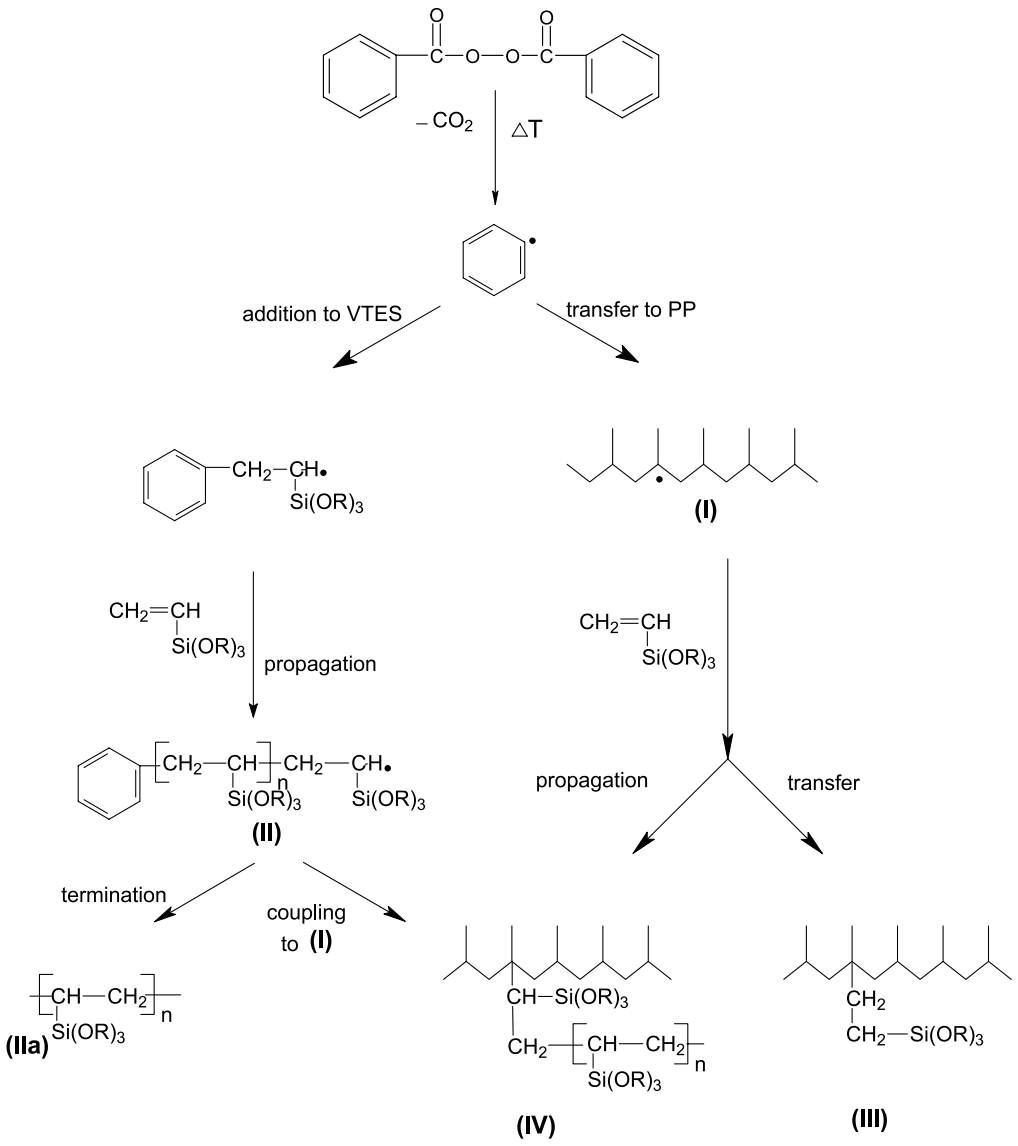

Scheme 1. Possible reactions for radical grafting of VTES on PP by initiation with peroxide during solid-state modification.

2.3. Characterization

2.3.1. Infrared (FT-IR) spectroscopy

BioRad Infrared Excalibur 3000 and FTS 6000 series infrared spectrometers were used for infrared analysis. The FTS 6000 series spectrometer coupled with an UMA500 microscope was used to characterize individual particles in ATR mode.

2.3.1.1. Attenuated total reflectance mode (ATR). Samples in powder form were characterized in reflectance mode with both instruments in the range of 4000–650 cm^{-1} with a resolution of 2 cm^{-1} and 100 scans. To characterize the inner part, particles were cut into two halves and selectively the outer and inner surfaces were measured using the microscope. The penetration depth of the evanescent wave is about 2–3 μm, while the thickness of a cut powder particle is about 500 μm. So, it can be assumed that the spectra correspond to the measured surfaces. The same argument holds for the outer surface characterization.

2.3.1.2. Transmission mode. To get an impression of grafting in bulk the powder samples were melt pressed to 50 μm films at 180 °C for about 10 min using a Collin compression press. Melt-pressed nanocomposites were characterized in transmission mode in the range of 4000–400 cm^{-1} with a spectral resolution of 4 cm^{-1} and 32 scans were co-added.

The calibration curve for quantitative analysis was constructed by recording FT-IR and solution ^{1}H NMR spectra of VTES-grafted PP with varying degrees of grafting. The degree of grafting (wt%) of VTES is calculated assuming that the grafted VTESS neither hydrolyzed nor homopolymerized. At least 10 different

specimens of the same sample were measured to ensure the repeatability and uniformity of the analysis.

2.3.2. Solution ^{1}H NMR spectroscopy

A Varian Gemini 300 MHz NMR spectrometer was used for solution ^{1}H NMR to construct the calibration curve for quantitative measurements using FT-IR spectroscopy. It is also useful in determining whether grafted monomers homopolymerize or form cross-links. Samples were prepared by dissolving grafted PP powder (~11.5 mg) in (~1 ml of) deuterated tetrachloroethane (with 1 mg DBPC stabilizer per 10 ml) at around 140 °C until a clear solution was obtained. All the measurements for modified PP were performed at 130 °C. In case of VTES and homopolymerized VTES, carbon tetrachloride was used as the solvent and reference, and measurements were done at room temperature. The number of moles of grafted VTES to PP was calculated by taking the ratio of the H-atoms of the ethoxy group (–O–CH_2–CH_3) of VTES to that of PP. Nanocomposites could not be characterized using solution NMR as they did not dissolve in any solvent, due to cross-linking during silica formation.

2.3.3. Magic-angle-spinning (MAS) ^{29}Si solid-state NMR spectroscopy

Magic-angle-spinning (MAS) ^{29}Si NMR was carried out on a Bruker DMX500 spectrometer operating at a ^{29}Si NMR frequency of 99 MHz and equipped with a 7-mm MAS probe head and the sample rotation rate was 4 kHz (2 kHz for liquids). About 2000 scans were accumulated. MAS ^{29}Si NMR was performed on nanocomposites powder to characterize the structure and the molecular connectivity of the cross-linked VTES and in-situ formed silica. The two-pulse sequence 90°-τ-180°-τ was used with a 90° pulse of 5 μs, an echo time 2τ of 15 μs, and an interscan delay of 180 s. The value of 180 s was chosen for practical reasons given the limited amount of measuring time. However, even at this relatively long interscan delay the ^{29}Si NMR spectra are not quantitative, as was evident from the line shape changes observed in a few test experiments at still longer interscans. The peak assignments for structure of silica is denoted by $Q^n = (RO)_{4-n}Si(OSi)_n$, as explained by Young et al. [29]. Assignments for various degrees of Si-atom substitution of the SiO_4 tetrahedra are reported elsewhere [30,31] The peaks are located within the following range of chemical shifts relative to TMS [$Si(Me)_4$]: $Q^4 = -106$ to -120 ppm, $Q^3 = -91$ to -101 ppm, $Q^2 = -74$ to -93 ppm and $Q^1 = -68$ to -83 ppm.

2.3.4. Size exclusion chromatography (SEC)

Molecular weights of VTES and its homopolymers were measured by size exclusion chromatography (SEC) at 40 °C using a Waters GPC equipped with a Waters model 510 pump, a model 410 differential refractometer (40 °C), a Waters WISP 712 auto-injector (50 μl injection volume), a PL gel (5 μm particles) 50×7.5 mm guard column and a set of two mixed bed columns (Mixed-C, Polymer Laboratories, 300×7.5 mm, 5 μm bead size, 40 °C). THF was used as the eluent at a flow rate of 1.0 ml/min. Calibration was carried out using narrow MWD polystyrene (PS) standards ranging from 600 to 7×10^6 g/mol. The molecular weight was calculated relative to the PS standards. Data acquisition and processing were performed using Waters Millenium 32 software.

2.3.5. High-temperature size exclusion chromatography (HT-SEC)

The molecular weight of PP in the nanocomposites was determined using high temperature SEC on a PL-GPC210 with 4 PL gel Mixed A Columns, a RALLS (light scattering) detector (Precision Detector, PD2040 at 800 nm), a H502 Viscometer (Viscotek), a refractive detector and DM400 data manager (Viscotek). The measurements were performed at 140 °C, using 1,2,4-trichlorobenzene as solvent and a narrow molecular weight PS standard as reference. The average of two independent measurements is reported.

2.3.6. Thermo-gravimetric analysis (TGA)

A Perkin–Elmer Pyris-6 TGA was used for quantitative determination of the in-situ formed silica and the grafted VTES on PP. It was also used to study the thermal stability of nanocomposites. Samples were heated under an oxygen atmosphere at 10 °C/min up to 900 °C and hold for 15 min to ensure complete oxidation of organic material. The residue is assumed to be silica due to complete oxidation. The moles of Si are calculated based on silica residue, from which moles of VTES or in-situ formed silica or grafted VTES-silica were determined.

2.3.7. Scanning electron microscopy (SEM)

A Philips field emission gun (FEG) environmental scanning electron microscope (ESEM) was used to determine the shape and size of in-situ formed silica particles. A qualitative measure of the particle size distribution was obtained from the SEM micrographs. In some cases (as described on the micrographs), the back-scattered emission (BSE) mode was used to get better contrast. For better focusing, a high electron voltage (viz. 1 eV) was used and samples were coated with carbon or platinum to avoid charging.

2.3.8. Transmission electron microscopy (TEM)

A Jeol JEM 2000 FX Transmission Electron Microscope (TEM) was used to characterize the morphology of the nanocomposites. The TEM was operated at 80 kV. Ultrathin sections of 50–70 nm were obtained at low temperatures (−40 °C) using a Reichert Ultracut E microtome, equipped with a diamond knife. The sections were not stained, since the electron density of the filler particles (silica) was much higher than matrix (PP). The effect of processing, such as extrusion or injection molding, on the morphology,

especially the dispersion of silica in the PP, was also investigated using TEM.

3. Results and discussion

The results of the chemical modification of PP and the sol–gel process are first discussed for a better understanding of the results of the actual PP-nanocomposites prepared via the combined SSM and the sol–gel process.

3.1. Solid-state modification (SSM)

The grafting of VTES is the most important aspect of the synthesis carried out via SSM. It controls the degree of adhesion between the matrix and the fillers. The following section discusses the reaction conditions for SSM and the reaction mechanism involved in the VTES grafting on PP, with special attention to the possibility of homopolymerization of VTES during grafting.

3.1.1. Reaction of vinyl silane with initiators (without PP)

A number of monomers, such as maleic anhydride [33,34], methacrylic acid [35,36] and vinylsilane (VTES) [36,37] have been used in previous SSM studies. These monomers upon grafting provide polarity and reactivity to PP. These were reported in these studies to be non-homopolymerizable monomers and were assumed to graft on PP as single monomeric units. In our study, VTES was chosen exactly for this reason.

However, SEC, ^{1}H NMR and MAS ^{29}Si NMR indicate that VTES, in the absence of PP, is susceptible to homopolymerization. VTES yields products with molecular weights as high as 50 kg/mol when initiated by BPO or AIBN (Table 1). The VTES monomer was recovered as such in the SEC analysis, indicating that cross-linking via –Si–O–Si– links formed upon hydrolysis with water present in THF (SEC solvent) and subsequent condensation of the VTES ethoxy groups did not occur. The high molecular weights observed with SEC, therefore, indicate true homopolymerization of VTES. ^{1}H NMR (Fig. 2(a)) indicates C=C to C–C conversion of approx. 40% upon homopolymerization of VTES using BPO as initiator. The appearance of a new peak around 1.6 ppm similar to that of the aliphatic H_{α} atoms in polyolefins suggests the formation of –CH– groups upon the polymerization of VTES. The conversion of C=C is in agreement with the amount of aliphatic –CH– groups formed. The VTES polymer was completely soluble in various solvents. This again excludes the possibility of cross-linking by hydrolysis and condensation of ethoxy groups. The MAS ^{29}Si NMR spectra in (Fig. 3) confirm the polymerization of VTES. The chemical shift of the Si-atom next to the C=C bond in VTES is -60 ppm. It represents the T^0 structure, where T^x corresponds to $Si(CH{=}CH_2)(OR)_{3-x}(O{-}Si{\equiv})_x$. If the Si-atom of this VTES is attached to a long saturated hydrocarbon chain, the ^{29}Si peak of the T^0 structure shifts to -45 ppm [38]. The MAS ^{29}Si NMR spectrum of the polymerized VTES in Fig. 3(b) indeed shows a new signal at -45 ppm. The spectrum shows no signals at the chemical shift positions of T^1, T^2 and T^3 structures, resulting from cross-linking via hydrolysis and condensation of the ethoxy groups.

The high molecular weight found with SEC, the appearance of a new peak at 1.6 ppm and the saturation of the C=C bonds visible in the ^{1}H NMR spectra, and the absence of any other signals than that of T^0 in the MAS ^{29}Si NMR spectra proves that VTES polymerizes along the vinyl unit. Based on these findings, a reaction mechanism for the grafting is proposed in Scheme 1. Part of the VTES may graft as monomeric unit on PP (structure III), similar to the grafting of maleic anhydride [33]. The other part of VTES grafted as monomeric unit on PP may then propagate to yield a polymer of VTES grafted on PP (structure IV). The other part of the VTES homopolymerizes (structure II) and may graft on the PP chain by coupling. The grafting of VTES involving homopolymerization is similar to that observed for styrene [16,25].

3.1.2. Optimum reaction parameters for grafting of VTES

Various time–temperature reaction schemes were followed for each free radical initiator. Temperature, rate of monomer addition, and initiator concentration were varied to optimize the reaction conditions. The effect of these parameters is shown in Fig. 4. The initiator concentration is expressed in wt% with respect to the amount of monomer. First, the degree of grafting increases rapidly with the increase in initiator concentration (up to 2 wt%) and is then followed by a more gradual increase (Fig. 4(a)). It is evident that a reasonable degree of grafting is achieved even at an initiator level of 2 wt%. At higher concentrations (ca. 4 wt%), β-scission of PP prevails [16], so 2 wt% initiator was used for further grafting experiments. The effect of the reaction temperature on the degree of grafting with different initiators is shown in Fig. 4(b). At a low reaction temperature, the rate of radical formation is too low resulting in a low final conversion. As the temperature is increased, the rate of formation of radicals and the rates of propagation and transfer increase, resulting in a higher degree of grafting. At even higher temperatures, however, too many radicals are formed in a given time interval which results in faster termination [39]. As a result, an optimum reaction temperature at which maximum grafting is achieved. Note that the optimum reaction temperatures

Table 1
Molecular weight (kg/mol) of polymerized VTES obtained by SEC

Initiator	M_n	M_w
LPO	6.4	13.1
BPO	8.8	17.4
AIBN	9.1	22.4
DTBP	17.0	68.7

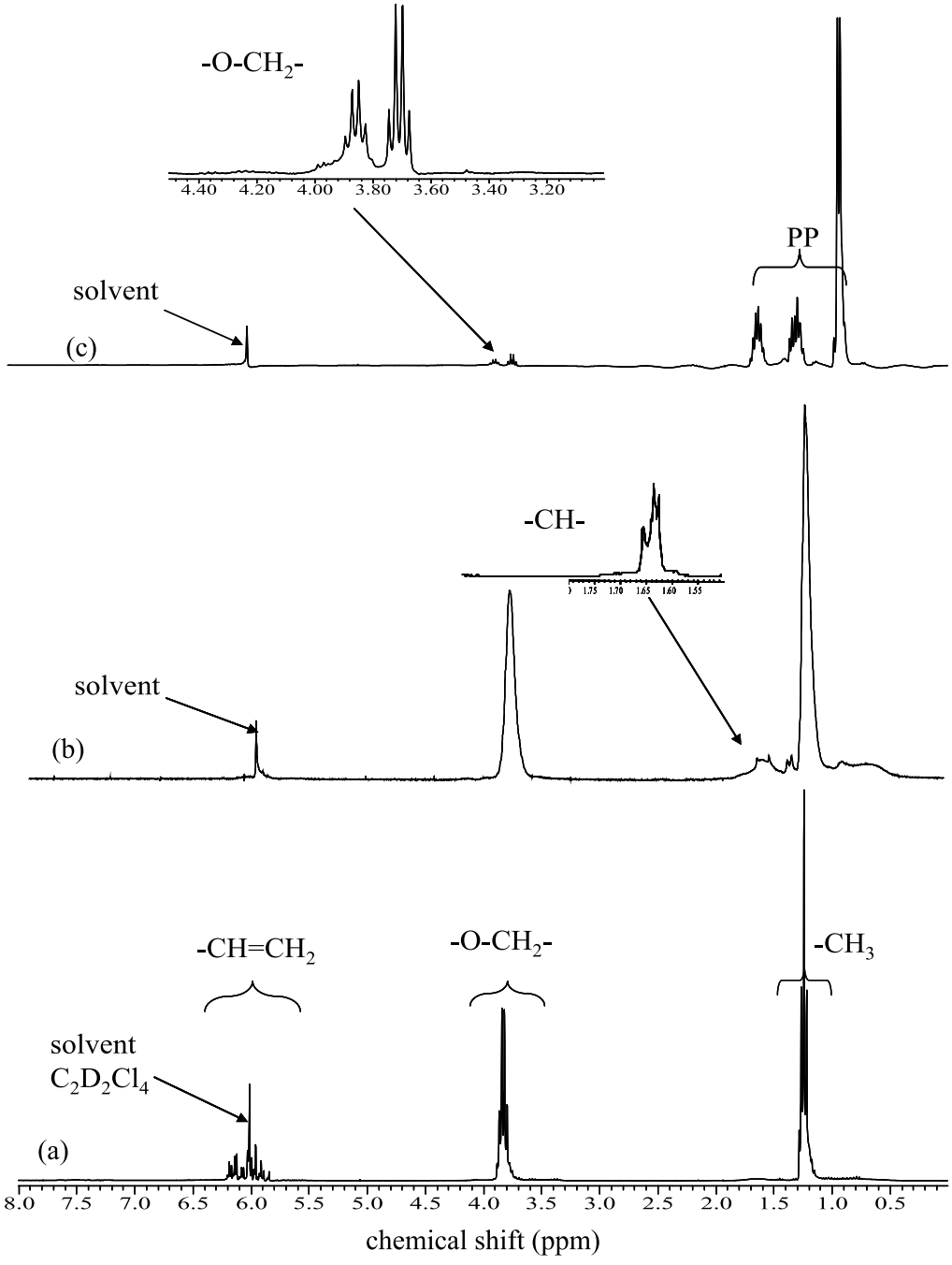

Fig. 2. ^{1}H NMR spectra of (a) VTES monomer, (b) VTES homopolymer, (c) PP-*g*-VTES monomer (13 wt%).

correspond to the temperatures at which initiators have half-life times of approx. 30 min (AIBN ~ 90 °C; BPO ~ 100 °C; LPO ~ 80 °C). A rate of addition of monomer of ~5 pph/min corresponding to the maximum grafting was used for all further reactions (see Fig. 4(c)). Using FT-IR microscopy, it was shown that the grafting of VTES on PP via SSM was uniform down to the level of 5 mg PP powder. Combining the ^{1}H NMR and FT-IR measurements, a calibration curve was constructed to calculate the degree of grafting. The degree of grafting is defined as wt% of vinyl silane per 100 gm of PP.

3.1.3. VTES grafting on PP

The structure of VTES-grafted PP was identified and the degree of grafting was quantified taking into account that VTES may homopolymerize during SSM. Fig. 2(c) shows the ^{1}H NMR spectra of PP with 13 wt% grafted VTES. The quartet at 3.76 ppm (the inset shows the magnified region of interest) indicate the presence of ethoxy groups attached to the Si-atom. Although no new peaks indicating the formation of aliphatic C–H groups were observed, the two quartets suggest two different structures and the broadening of peaks indicate that

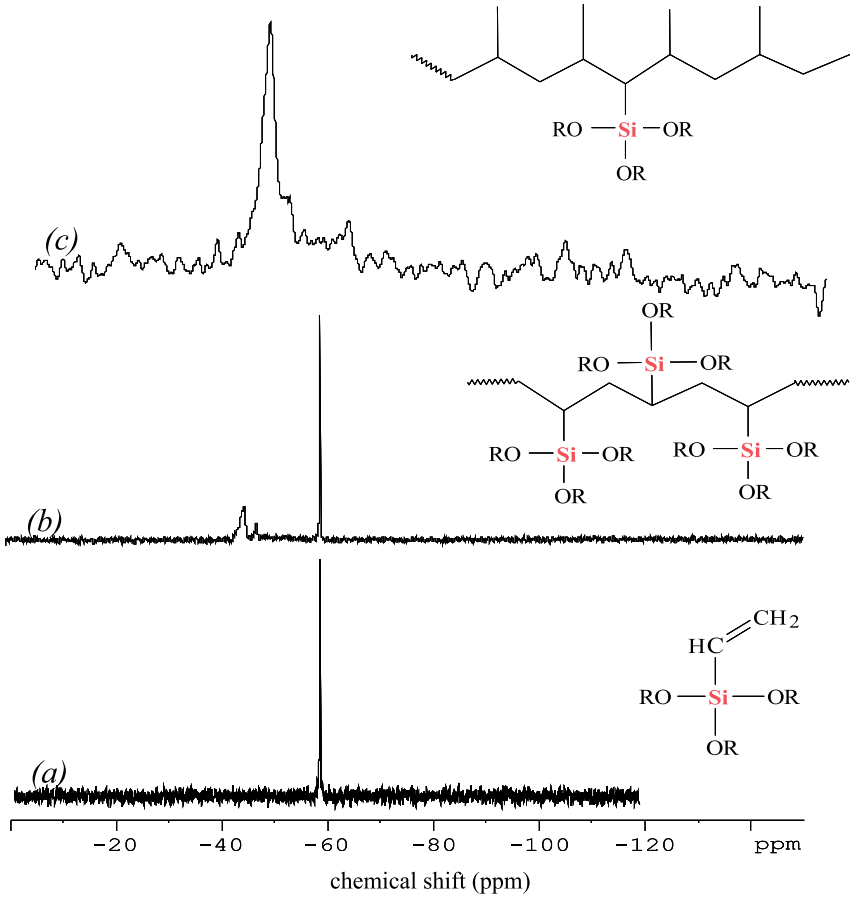

Fig. 3. MAS ^{29}Si NMR spectra of (a) VTES monomer, (b) VTES homopolymer, (c) PP-*g*-VTES monomer (10 wt%).

VTES may have grafted as a polymer. No resonances of vinyl H-atoms were observed (6 ppm), implying that there is no unreacted monomer in the grafted PP. The MAS ^{29}Si NMR spectra in Fig. 3(c) of modified PP confirm the presence of grafted VTES. When VTES is attached to a long hydrocarbon chain, the ^{29}Si peak of the T0 structure shifts to ~ -45 ppm [38]. Therefore, the peak at -45 ppm in the spectrum can be assigned to VTES grafted on PP backbone. The susceptibility of VTES to homopolymerize as explained earlier, however, does not rule out the possibility of VTES grafting as monomer as well as polymer to PP.

The PP pores are a few micrometers in size and can act as mini-reactors inside the PP-macroparticles, in which VTES can be dispersed and homopolymerize. The VTES can diffuse in the pores of PP or even in the amorphous phase of PP and may graft or homopolymerize there. The solubility parameter of PP is 7.43 $(cal/cc)^{1/2}$ and that of VTES is 8.0 $(cal/cc)^{1/2}$, so it is expected that the VTES can be absorbed in the amorphous phase of PP during solid-state

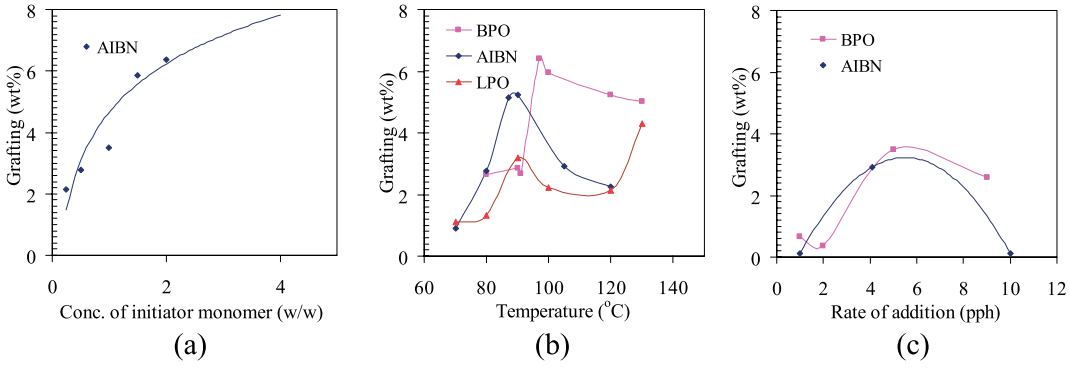

Fig. 4. The influence of the reaction conditions on the grafting efficiency: (a) effect of initiator concentration ($T=90$ °C), (b) effect of temperature (2 wt% initiator), (c) effect of rate of addition (2 wt% initiator). The curves are used to indicate the trend.

modification. Moreover, the grafting can take place at the interface between VTES-filled pores and PP, i.e. at the PP surface. However, we found that grafting during SSM mainly takes place in the amorphous phase of PP. ^{1}H spin lattice relaxation times in the rotating frame, $T_{1\rho}\{H\}$, were measured for the amorphous and crystalline phase of PP via cross polarization to ^{13}C and ^{29}Si nuclei in the solid-state. $T_{1\rho}\{H\}$ for the crystalline and amorphous phase of the original PP were found to be 35 and 4 ms, respectively. In case of VTES-grafted PP, it was found that $T_{1\rho}\{H\}$ for the grafted VTES was also around 4 ms, indicating that grafting took place in the amorphous phase of PP. This restricts the chances of homopolymerization of VTES, since the diffusion of the monomer is limited by the absorption in the amorphous phase of PP.

The FT-IR spectrum in Fig. 5 illustrates the grafting of VTES on PP via SSM. The band assignment details are given in Table 2. The strong Si–O–C stretching [40] vibration bands at 1120 and 1080 cm^{-1} accompanied by a shoulder at 950 cm^{-1} are indicative for the grafting of VTES on PP. The band at ~1600 cm^{-1}, corresponding to vinyl groups CH=CH_2 of VTES, is absent, so no unreacted monomer is present. The cumulative area under the 1120 and 1080 cm^{-1} peaks is considered to be proportional to the amount of grafted VTES. The area of –CH_3 rocking band of PP at 899 cm^{-1} was used as reference.

The overlapping of various bands in the FTIR-spectrum assigned to the H-atoms attached to different carbons and the similarity in the structures formed make it difficult to identify whether VTES is grafted as monomer or polymer on the PP backbone. The rapid transfer of the tertiary hydrogen abstracted from PP to the free VTES radical may prevent the homopolymerization of VTES during modification of PP via SSM as explained by Rätzsch et al. for grafting of maleic anhydride in the concentration regime of our interest [16]. This may suggest that VTES is grafted as a single monomeric unit on PP. The combined results from ^{1}H NMR and MAS ^{29}Si NMR on modified PP via SSM show that VTES is grafted as monomer on the PP backbone, even though VTES was found to homopolymerize by a free radical reaction mechanism in the absence of PP. No homopolymer of VTES was found in the pores of PP and, $T_{1\rho}\{H\}$ experiments showed that VTES is present in the amorphous phase of PP. Therefore, VTES is most likely grafted as a monomeric unit on PP (structure III shown in Scheme 1) in the concentration range of VTES used for SSM.

3.1.4. Cross-linking of grafted monomer

The cross-linking of VTES-grafted PP proceeds through hydrolysis and condensation of grafted VTES. In presence of water, the ethoxy groups attached to Si-atom undergo hydrolysis and upon condensation form –Si–O–Si– links thus cross-linking two grafted PP chains. The FT-IR spectrum in Fig. 5 shows the splitting of the bands at 1040 and 1080 cm^{-1} originating from the stretching of linear (aliphatic) Si–O–Si linkages formed during cross-linking [41]. The shift of transverse optical (νTO) components towards a lower wavenumber also indicates the presence of linear structures [42] as in cross-links. The 950 cm^{-1} band from Si–O–CH_2CH_3 stretching vibrations disappeared due to hydrolysis. Water treated VTES-grafted PP did not dissolve in commonly used good solvents for PP, such as xylene, toluene, tri-chlorobenzene, even when heated up to temperatures as high as 200 °C, which is another indication that grafted VTES formed cross-links between the PP chains.

3.2. Hybridization (sol–gel reaction)

The sol–gel reaction is an important step for making inorganic nanofillers in the pores of PP. The rate of formation and size of silica hybrid particles was controlled by variation of the pH of the HCl/water (acidic) or NH_4OH/water (basic) systems, which trigger the hydrolysis and condensation reactions. At high pH, solubility of small particles is higher than at low pH, resulting in larger particles (5–10 nm). Under basic conditions, particles are negatively charged and hence repel each other. Therefore, they do not collide and are stable as such, while under acidic conditions the charge of repulsion is reduced and aggregation occurs, resulting in a branched network of silica particles of (2–4 nm) [43,44]. Fig. 6 shows the SEM micrographs of the silica particles prepared under different

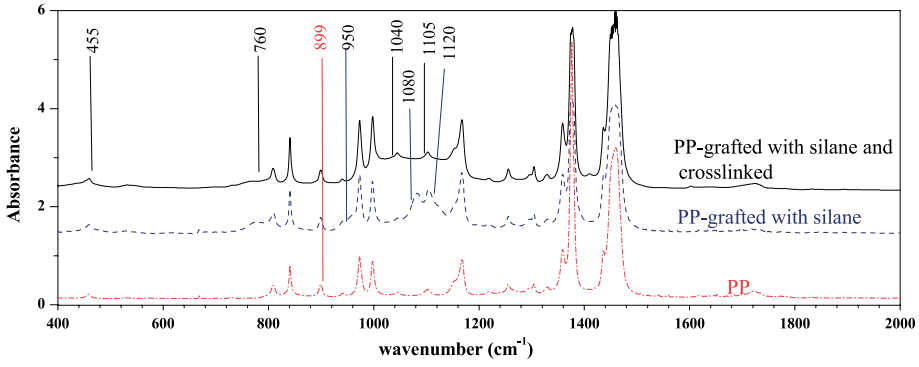

Fig. 5. FT-IR spectra of silane-grafted PP and cross-linked silane-grafted PP.

Table 2
Assignments of infrared bands in the FT-IR spectra [35,43]

Assignment	Wavenumber (cm^{-1})
Stretching ν Si–O–C	1120
Stretching ν_{as} Si–O–Si	1080
ν_1 (LO)[a]	~1207
ν_2 (LO)	~1160
ν_3 (TO)[b]	~1085
ν_4 (TO)	~1068
Stretching ν_s Si–O–R (R–H; C_2H_5)	950–980
Stretching ν_s Si–O–Si	800
Rocking ρ $-CH_3$ of PP	899
Stretching ν –O–H	2500–3800

[a] Longitudinal optical.
[b] Transverse optical.

catalytic conditions in the absence of PP. It is evident that the size of silica particles formed is in close agreement with the results from literature. In view of this, we used base catalyst conditions for in-situ preparation of silica in the pores of PP.

3.3. Chemical and structural characterization of nanocomposites

3.3.1. PP/silica nanocomposites

Next, silica nano-clusters were formed in-situ in the pores of isotactic PP through the sol–gel method. The FT-IR spectra depicted in Fig. 7 are of pure silica (in the absence of PP) prepared by the sol–gel method and of PP/silica nanocomposites under the same reaction conditions. The strong and broad peaks around 1000–1100 cm^{-1} can be attributed to Si–O–Si linkages. Fidalgo et al. [42] discussed the structural defects of sol–gel derived silica in the presence of polymers in detail. The intermediate frequency band at ~800 cm^{-1} involves the symmetric stretching vibration of the Si–O–Si atoms (ν_s Si–O–Si). The dominant band near 1080 cm^{-1} can be assigned to asymmetric stretching vibrations of Si–O–Si atoms (ν_{as} Si–O–Si) of nearly perfect silica structures with cyclic Si–O–Si (Table 2). This dominant band at 1080 cm^{-1} can be observed in both spectra, which implies the formation of silica clusters in the pores of PP. The bands are slightly shifted in the presence of PP as was also explained by Fidalgo et al. The 1080 cm^{-1} peak is usually split into two components as a result of long range coupling interactions: a transverse optical (TO) and a longitudinal optical (LO). The shoulder associated with this band, centered at ~1150 cm^{-1}, has been usually related to the LO component and the band nearing 1070 cm^{-1} to TO component [45,46]. The shift towards higher wavenumbers of the TO and LO components of in-situ formed silica in the PP pores compared to that of pure silica is related to a decrease in the porosity of the silica formed [42]. There is no appreciable increase in relative intensities of the peaks at ~1207 and 1090 cm^{-1}, which indicates that the in-situ formed silica is similar to that formed by the sol–gel method without PP. Moreover, the relative intensity of the ν_sSi–OH band (~950 cm^{-1}) in the case of pure silica and in-situ

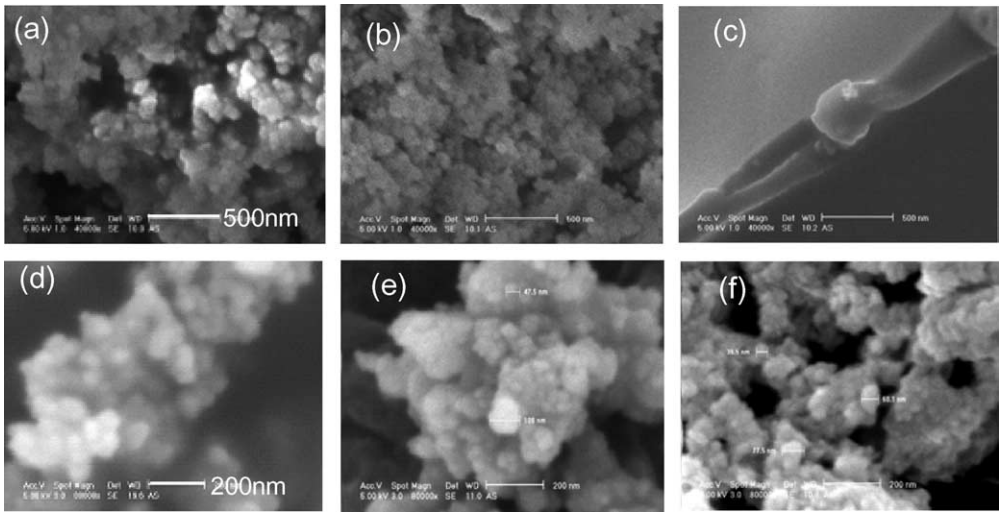

Fig. 6. SEM micrographs of silica prepared by the sol–gel method: (a) no catalyst (~80 nm) (b) base catalyst: pH = 10 (~50 nm) (c) acid catalyst (≤10 nm). After oxidation in TGA: (d) silica prepared as such, (e) PP/silica nanocomposites, (f) PP-*g*-silane/silica nanocomposites.

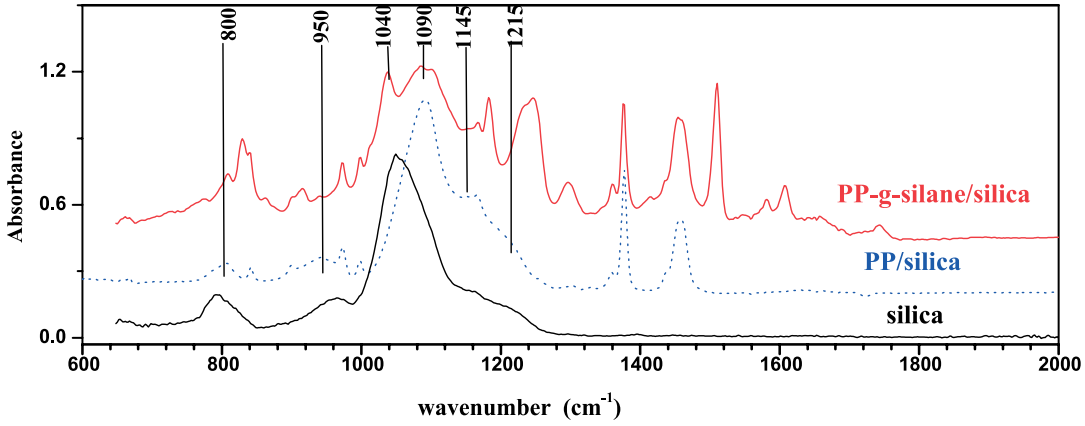

Fig. 7. FT-IR spectra of silica by the sol–gel method as such and in-situ formed silica in PP and silane-grafted PP.

formed silica in PP is comparable, indicating a similar extent of condensation in both cases. These peaks also imply that some hydroxy groups are still present on the outer surface of the silica particles. All these results demonstrate the formation of less porous, more constrained (4-fold) siloxane ring structures of silica with some hydroxy groups on the surface.

The MAS ^{29}Si NMR spectra of the sol–gel derived silica and in-situ formed silica-clusters in PP are shown in Fig. 8. The band at −112 ppm, assigned to the Q^4 structure, indicates fully condensed silica (SiO_2), while the peak observed at −104 ppm is assigned to a Q^3 structure with a Si-atom connected to three Si and one H or C atom in the second coordination sphere. The high intensity of the Q^3 band suggests a large surface area with –OH or –OR groups which is in agreement with FT-IR results. There are no

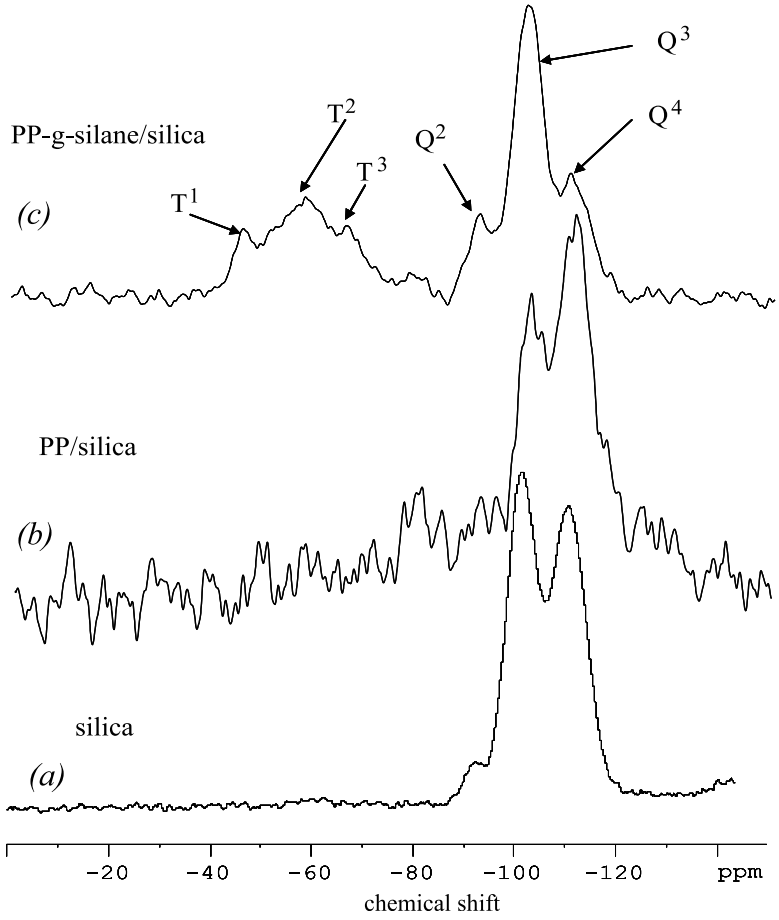

Fig. 8. MAS ^{29}Si NMR spectra of (a) silica, (b) PP/silica, (c) PP-*g*-silane/silica nanocomposites.

peaks related to Q^1 and Q^2 structures in the spectra, indicating that the condensation reaction during the sol–gel reaction is fairly complete. The structure of in-situ formed silica (Fig. 8(b)) is close to the separately prepared silica (Fig. 8(a)), suggesting that the presence of PP does not affect the structure formation of silica, as in agreement with the FT-IR measurements. The extremely long ^{29}Si spin–lattice relaxation time of Q^4 structures makes a quantitative analysis difficult, especially when the silica particles are enclosed in the PP matrix.

3.3.2. PP-g-silane/silica nanocomposites

The FT-IR spectrum in Fig. 7 also shows the chemical structure of silica synthesized in-situ in the VTES-grafted PP. The spectra of PP/silica and PP-*g*-silane/silica nanocomposites show the effect of grafting on the chemical structure of silica. The peak at 1060 cm^{-1} assigned to the linear Si–O–Si linkage has shifted towards a lower wavenumber (1040 cm^{-1}) in the spectrum of PP-*g*-silane/silica. The peak at 1090 cm^{-1}, attributed to the Si–O–C stretching vibrations, has broadened. The broad shoulder at $\sim$1200 cm^{-1}, assigned to νLO, is very weak. All these observations suggest that the grafted VTES takes part in the in-situ silica formation. The MAS ^{29}Si NMR spectra in Fig. 8(c) shows the structure of silica particles formed in the VTES grafted PP. The grafted VTES (-45 ppm) evolves in the presence of water and TEOS into T^0 and T^1 structures. The *Q*-type structures ($Q^2\sim-92$ ppm; $Q^3\sim-101$ ppm; $Q^4\sim-112$ ppm) in the spectrum are assigned to the in-situ formed silica. From ^{1}H NMR, FT-IR and MAS ^{29}Si NMR, it can be inferred that grafted VTES becomes part of in-situ formed silica. Pre-modification of PP gives better control over adhesion between matrix and in-situ formed nanosilica. Grafted VTES has become part of the in-situ formed silica and, hence, will result in a strong chemical interaction with the polymer matrix.

3.4. Efficiency of silane grafting and silica formation

Table 3 shows the comparison of the data obtained through the various techniques used to quantify VTES grafting and the silica formed in the pores of PP. The results from TGA, elemental analysis and ^{1}H solution NMR are consistent, confirming the validity and reliability of these methods to quantify the composition of the nanocomposites. For VTES grafted on PP via SSM, the plot of grafted VTES versus concentration of monomer added shows that the degree of grafting increases initially and forms a plateau above a certain concentration of VTES (see Fig. 9(a)). Other researchers observed a similar behavior for the grafting non-homopolymerizable monomers [47,48]. The initial increase in grafting efficiency can be attributed to the increased availability of monomers at active PP radical sites with increasing monomer concentration. The solubility of VTES in the amorphous phase determines the grafting efficiency. The grafting efficiency did not decrease at higher concentrations of VTES, although this is commonly observed in easily homopolymerizable monomers such as styrene [16].

Table 3
Comparison of amount of monomers grafted/incorporated in iPP after solid-state modification by various analytical methods (wt% is expressed per 100 g of PP)

TEOS (wt%)	VTES (wt%)	TGA (wt%)	Elemental analysis (wt%)	^{1}H NMR (wt%)
10	0	2.2		
15	0	4.8	5.8	
20	0	6.5	6.9	
30	0	10.1	10.7	
0	15	1.6		1.5
0	18			2.8
0	20			3.7
0	25	4.2		4.3
10	15	3.6		
15	15	7.4	7.4	
15	20	8.7	8.0	
20	15	6.2		

In the case of the PP/silica nanocomposites the amount of TEOS converted to silica increased with increasing TEOS concentration. Unlike the grafting of VTES on PP, which takes place only in the amorphous phase of PP, silica can be formed in the pores too and is not necessarily restricted to the amorphous phase of PP. So, the efficiency of silica formation remained constant irrespective of the TEOS concentration as seen in Fig. 9(b). A similar trend was observed for the PP-*g*-silane/silica nanocomposites, in which silica particles are formed in the VTES-grafted PP. Fig. 9(b) shows the amount of silica formed in VTES-grafted PP as a function of the amount of TEOS added. For simplicity, only data for 2 wt% VTES-grafted PP are shown. It is suggested that grafted VTES does not affect the formation of silica.

3.5. Molecular weight of PP in nanocomposites after SSM

Table 4 shows the molecular weight of VTES-grafted PP via SSM and PP in nanocomposites determined using high temperature SEC. The data indicate that no molecular degradation occurred during SSM. The most likely reason is drop in the rate of β-scission by 5 orders of magnitude as the reaction temperature is reduced from 250 °C as used in melt

Table 4
Molecular weight of PP nanocomposites (kg/mol) using high temperature SEC

Sample	M_n	M_w
PP as received	106	382
PP+silica (2.5 wt%)	106	387
PP-*g*-silane (2 wt%)	100	303
PP-*g*-silane (5 wt%)	106	357
PP-*g*-silane (10 wt%)	115	325

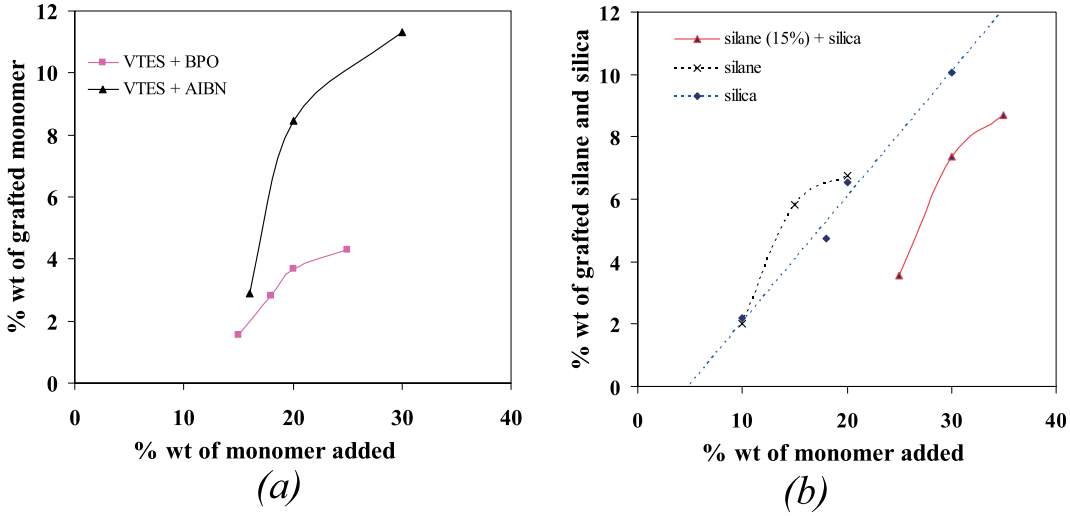

Fig. 9. Plots of (a) silane grafted on PP and (b) in-situ formed silica in pores of PP.

modification to 100 °C for SSM as reported by Rätzsch et al. [19]. In addition, the inert nitrogen atmosphere used during the reaction prevents the oxidative degradation.

Based on this, we propose the reaction mechanism as shown in Scheme 1, in which we assert that grafting of PP with VTES might proceed according to a simple 'chain transfer mechanism'. The reaction temperature used in the present study is 110 °C, which is lower as compared to 150 °C used in earlier studies [16,49]. This may also have an effect on the molecular weight and the grafting efficiency. In some of these earlier studies, the grafting mechanism for SSM for similar monomers, such as maleic anhydride (MAH)-grafted PP, was proposed based on products of PP grafted in the melt. It was suggested that the grafting reaction takes place after PP chain scission; this assumption was further sustained by the remarkable decrease in molecular weight of the solid-state grafted PP. However, we did not observe such a behavior. This shows that SSM is advantageous over melt modification process.

3.6. Structure and morphology of nanocomposites

The dispersion of the in-situ formed silica particles and their size and shape are the most important factors affecting the properties of nanocomposites. The morphology of nascent PP powder before modification is also important in that respect. As described earlier, the size of silica particles can be varied depending on the catalyst used. The base catalyst was used for the synthesis of the PP nanocomposites. ATR FT-IR microscopy was used, along with SEM and TEM, to study the dispersion of in-situ formed silica before melt processing the nanocomposites.

3.6.1. PP/silica nanocomposites

The FT-IR spectra depicted in Fig. 10(a) are from the outer and inner surface of PP/silica nanocomposite macro-particles. It is evident that the formation of silica is uniform throughout the macroparticle of PP. TEOS, when mixed with PP powder, dispersed throughout the particle due to surface tension and capillary effect in the channels. When water is added in the presence of a catalyst the sol–gel reaction proceeds in these channels and at the surface.

3.6.2. PP-g-silane/silica nanocomposites

Fig. 10(b) shows the FT-IR spectrum of VTES-grafted PP powder taken from the reactor and vacuum dried to remove unreacted VTES. The PP powder was characterized in the same way as described above. It is evident that VTES is grafted not only near the surface but also deep in the powder particle. The spectra indicate that grafting is more inside than on the surface (see peaks at 1080 and 1105 cm^{-1}). This may be due to the higher surface tension of VTES and the capillary effect of the pores and preferential absorption of the monomer in the amorphous phase of PP. Also, the grafting reaction is carried at higher temperatures than hybridization, which enhances the diffusion of monomer into the pores.

Fig. 10(c) shows that the in-situ formed silica-particles are uniformly distributed in the modified PP as well. The grafted VTES may act as nucleus for the growth of silica as observed by Young et al. in the case of the Surlyn-silica system [29]. As described earlier, the grafted VTES indeed becomes part of silica and may be the point of adhesion between PP and in-situ formed silica.

3.6.3. Shape, size and size distribution of in-situ formed silica particles in PP

The morphology as observed by TEM shows a narrow distribution of particle size of silica as shown in Fig. 11. The particle size near the surface and the center of the PP macroparticle were found to be similar. Fig. 11(a) and (b) gives a magnified view of the in-situ formed silica at the edge and in the center of the PP macro-particle respectively. Silica nano-clusters formed at the edge (ca. 30–100 nm) are

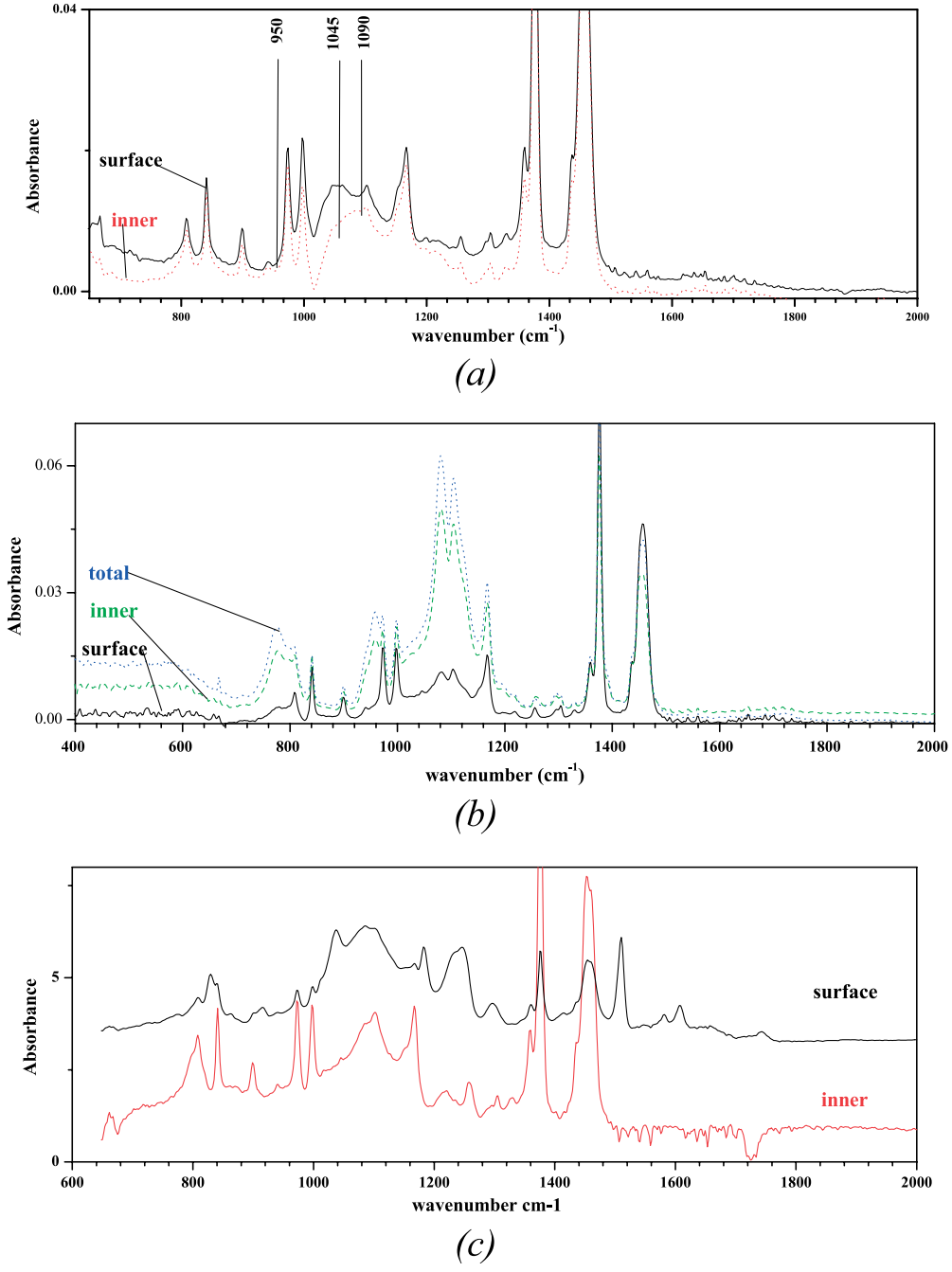

Fig. 10. FT-IR spectra (in ATR mode) showing the inner and outer surfaces of (a) PP/silica, (b) silane-grafted PP, (c) PP-*g*-silane/silica nanocomposites.

same as those inside the macroparticle PP (ca. 50–100 nm). The morphology of these nanocomposites was stable even after mixing in a mini-extruder screw extruder. Fig. 11(c) shows the silica nano-clusters formed in PP-*g*-silane/silica nanocomposites. The size and shape of silica formed is comparable to that formed in PP/silica nanocomposites. The size and structure of silica particles formed in the PP were also confirmed by oxidation of the nanocomposites in TGA at 800 °C. The residue from TGA was characterized with SEM. Silica particles synthesized in the absence of PP were also oxidized to check the effect of oxidation on the particles. Comparing Fig. 6(a) and (d) (before and after oxidation, respectively), we observe that the oxidation of silica does not affect the sizes and the structure of primary particles. Therefore, it can be assumed that oxidation does not affect the structure of in-situ formed silica in PP. Fig. 6(e) and (f) shows the silica formed in PP/silica and PP-*g*-silane/silica nanocomposites with typical sizes of 50–100 nm after oxidation. The morphologies of PP/silica nanocomposites observed by SEM before and after oxidation and ATR FT-IR microscopy measurements indicate that the silica-particles are dispersed throughout

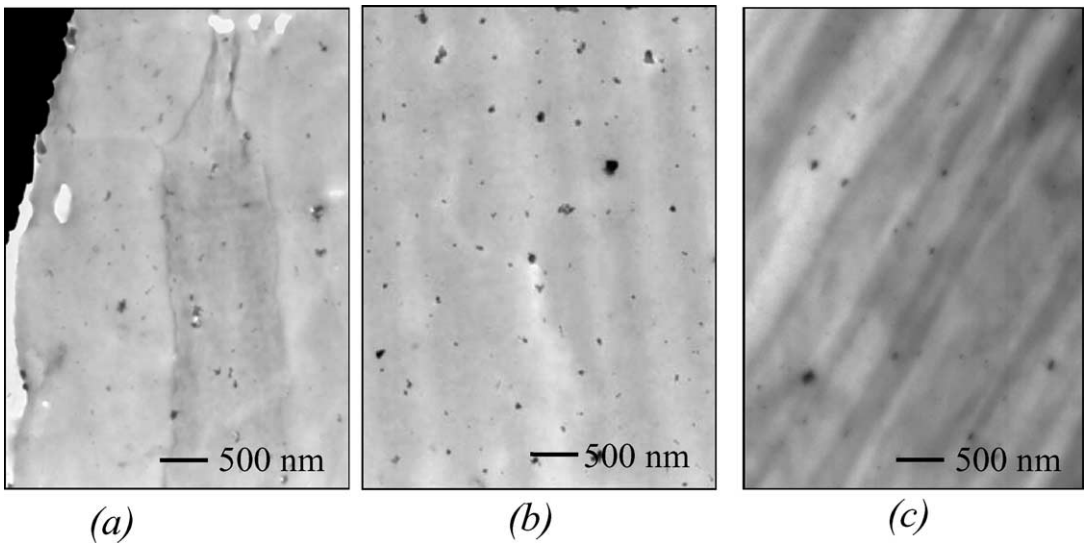

Fig. 11. TEM micrographs of (in-situ formed) PP/silica nanocomposite (5% of silica): (a) edge, (b) center and (c) PP-*g*-silane/silica nanocomposites.

the PP macroparticles with a size distribution between typically 50–150 nm.

4. Conclusions

PP-nanocomposites with and without chemical linkage between the silica particles and the PP matrix were synthesized by a new approach combining SSM with VTES and a sol–gel method with the idea that grafted monomeric VTES is incorporated in the silica during the sol–gel reaction to control the interaction. Bulk polymerization experiments with the same experimental conditions as in SSM showed that homopolymerization of VTES to high molecular weight occurs but at limited conversions, suggesting that VTES can be grafted on PP as monomer or polymer or both. However, ^{1}H NMR, MAS ^{29}Si NMR and FT-IR spectroscopy studies demonstrated that VTES graft on PP as a single monomeric unit which is subsequently incorporated in in-situ formed silica. $T_{1\rho}\{H\}$ measurements via cross polarization to the ^{13}C and ^{29}Si nuclei in solid-state indicated that VTES was mainly absorbed and subsequently grafted in the amorphous phase of PP and not at the VTES-filled pore-PP interface. The ATR-FTIR microscopy results of PP macroparticles suggested that VTES is grafted not only on the surface of PP macro-particles but also inside the macro- and sub-particles. In situ formed silica is also formed throughout the PP particle. No molecular degradation of PP was observed in the nanocomposites and the degree of grafting was comparable to grafting in the melt. MAS ^{29}Si NMR showed that the silica-like clusters are predominantly Q^3 and Q^4 type, indicating that the in-situ formed clusters are highly condensed with some hydroxy groups at the surface. Particles of 50–150 nm with a near-spherical shape were observed by TEM and SEM. The observation that silica particles are uniformly dispersed proves that the new approach is advantageous over conventional methods. These systems may used as model systems for investigating the mechanism of toughness enhancement of semi-crystalline polymers, and more specifically of PP.

Acknowledgements

The authors acknowledge the help given by Anne Spoelstra and Pauline Schmit with SEM and TEM characterization. The authors are also grateful to Otto van Asselen for the discussion and interpretation of FT-IR measurements. This study is financed by DPI project No 133.

References

[1] Gilman JW, Jackson CL, Morgan AB, Harris Jr R. Chem Mater 2000; 12:1866.
[2] Kojima Y, Usuki A, Kawasumi M, Okada A, Fukushima Y, Kurauchi T, et al. J Mater Res 1993;8:1185.
[3] Messersmith PB, Giannelis EP. J Polym Sci, Polym Chem 1995;33: 1047.
[4] Vaia RA, Price G, Ruth PN, Nguyen HT, Lichtenhan J. J Appl Clay Sci 1999;15:67.
[5] Garcia-Lopez D, Picazo O, Merino JC, Pastor JM. Eur Polym J 2003; 39:945.
[6] Koo CM, Kim JM, Choi MH, Kim SO, Chung IJ. J Appl Polym Sci 2003;88:1526.
[7] Giannelis EP, Krishanmoorti RK, Manaias E. Adv Polym Sci 1998; 138:107.
[8] Alexandre M, Dubois P. Mater Sci Eng R 2000;28(1):1.
[9] Thio YS, Argon AS, Cohen RE, Weinberg M. Polymer 2002;43:3661.
[10] Jancar J, Kucera J. Polym Eng Sci 1990;30:707.
[11] Van Es M. PhD Thesis Technische Universiteit Delft, The Netherlands; 2001.
[12] Kato M, Usuki A, Okada A. J Appl Polym Sci 1997;66:1781.
[13] Usuki A, Kato M, Okada A. J Appl Polym Sci 1997;67:137.
[14] Kurokawa Y, Yasuda H, Oya A. J Mater Sci Lett 1996;15:1481.

[15] Ray SS, Okamoto M. Prog Polym Sci 2003;28:1539.
[16] Rätzsch M, Arnold M, Borsig E, Bucka H, Reichelt N. Prog Polym Sci 2002;27:1195.
[17] Rangarajan R, Paramaeswaran VR, Lee S, Rinaldi VM. Polymer 1990;31:1703.
[18] Rangarajan R, Lee S. US Patent US5079302; 1992.
[19] Rätzsch M, Bucka H, Hesse A, Arnold M. J Macromol Sci Pure 1996; A33:913.
[20] Cecchin G. Symposium proceeding of polypropylene past present and future: the challenge continues; Ferrara 1998. p. 25–51.
[21] Special issue: Organic–inorganic Nanocompos Mater Chem Mater 2001;10:13.
[22] Wen J, Wilkes GL. Chem Mater 1996;8:1667.
[23] Ellsworth MW, Novak BM. J Am Chem Soc 1991;113:2756.
[24] Kim KD, Kim HT. J Sol–gel Sci Technol 2002;25:183.
[25] Picchioni F, Goossens JGP, van Duin M, Magusin P. J Appl Polym Sci 2002;89:3279.
[26] DeNicola AJ, Guhaniyogi S. EP Patent EP0439079; 1991.
[27] Roelands D., Graduation report, Technische Universiteit Eindhoven, The Netherlands; 1999.
[28] Xanthos M, Biesenberger JA. Reactive extrusion: principles and practice. Munich: Hanser Publication; 1992. p. 102–109.
[29] Young SK, Jarrett WL, Mauritz KA. Polymer 2002;43:2311.
[30] Qui G, Tang ZL, Huang NX, Gerking L. J Appl Polym Sci 1998;81: 294.
[31] Otocka EP, Kwei TK, Salvoey R. Macromol Chem Phys 1969;129: 144.
[32] Mauritz KA, Warren R. Macromolecules 1989;67:1799.
[33] Mulder FM, Heinen W, van Duin M, Lugtenburg J, de Groot HJM. Macromolecules 2000;33:5544.
[34] Yu J, He J. Polymer 2000;41:891.
[35] Lazar M, Hrckova L, Fiedlerova A, Borsig E, Rätzsch M, Hesse A. Die Angew Makromol Chem 1996;243:57.
[36] Ivanchev SS, Rätzsch M, Mesh AM, Khaikin SYa, Bucka H, Hesse A, et al. Polym Sci Ser B 2001;43:85.
[37] Sheish YT, Tsai TH. J Appl Polym Sci 1998;69:255.
[38] Shimojima A, Umeda N, Kazuyuki K. Chem Mater 2001;12:3610.
[39] Odian G. Principles of polymerization. 4th ed. Hoboken: Wiley-Interscience; 2004.
[40] Siuzdak DA, Mauritz KA. J Polym Sci, B: Phys 1999;37:143.
[41] Mauritz A. Mater Sci Eng C-Biol S 1998;6:121.
[42] Fidalgo A, Ilharco LM. J Non-Cryst Solids 2001;283:144.
[43] Mark JE, Pen JS. Macromol Rapid Commun 1982;3:681.
[44] Brinker CJ, Schere GW. Sol–gel science—the physics and chemistry of sol–gel processing. London: Academic Press; 1990.
[45] Galeener FG. Phys Rev B 1979;19:4292.
[46] Almeida R, Guiton T, Pantano C. J Non-Cryst Solids 1998;109:433.
[47] Li Y, Xie XM, Guo BH. Polymer 2001;42:3419.
[48] Machoda AV, van Duin M, Covas JA. J Polym Sci, Polym Chem 2000;38:3919.
[49] Borsig E, Hrckova L, Fiedlerova A, Lazar M. J Macromol Sci Pure 1998;35:1313.